Applied Water Science (2024) 14:92
https://doi.org/10.1007/s13201-024-02152-z

ORIGINAL ARTICLE

Metronidazole adsorption by bio-synthesized silver-zinc ferrite nanoadsorbent in presence of chitosan from aqueous media: response surface methodology

Saeed Rajabi[1,2] · Zahra Derakhshan[1,3] · Majid Hashemi[4,5] · Mehrzad Feilizadeh[6] · Saeed Heidari Kochaki[6] · Hassan Hashemi[1,2] · Mohammadhossein Salehi[1,3] · Amirreza Zare[1,3] · Narges Sadat Shourabi[1,3] · Saeideh Moradalizadeh[4,5]

Received: 4 December 2023 / Accepted: 7 March 2024

Abstract

A novel magnetic biocomposite adsorbent, denoted as $AgZnFe_2O_4$@Ch, was utilized for the degradation of Metronidazole (MNZ) from water. Various analytical techniques, including vibrating sample magnetometer (VSM), X-ray diffraction (XRD), Brunauer–Emmett–Teller, Fourier transform infrared spectroscopy, and field emission scanning electron microscopy (FESEM), were applied to investigate the characteristics of the magnetic biocomposite adsorbent. XRD examination confirmed the formation of spinel ferrites phases. FESEM assessment indicated a notable reduction in sample aggregation. The ferromagnetic character of the adsorbent was well demonstrated by VSM analysis. The saturation magnetization value for straightforward separating by the outside magnetic fields was 14.64 emu/g. An analytical modeling approach was used to evaluate and analyze the impacts of factors including MNZ initial concentration, temperature, contact time, adsorbent dosage, and pH. Optimized conditions involved an adsorbent dosage of 0.9 g/L, pH of 7, MNZ initial concentration of 10 mg/L, and a contact time of 50 min, resulting in a peak adsorption efficiency of 65.53% under favorable circumstances. A good degree of fit was achieved with the linear model. The experimental equilibrium data fitting to the Langmuir, Freundlich, and Temkin isotherm models demonstrates that the Langmuir model was an effective and appropriate model for evaluating adsorption. Intraparticle kinetic modeling was also shown to be better suitable for characterizing the MNZ adsorption onto the adsorbent. The thermodynamic analysis indicated that the process of MNZ adsorption by $AgZnFe_2O_4$@Ch was characterized by exothermicity and lacked spontaneity.

Keywords Metronidazole · Adsorbent · Bio-synthesize · Chitosan · Characterization

✉ Zahra Derakhshan
derakhshz@sums.ac.ir

✉ Mehrzad Feilizadeh
m.feilizadeh@shirazu.ac.ir

Saeed Rajabi
saeedrajabi27@gmail.com

Majid Hashemi
mhashemi120@gmail.com

Hassan Hashemi
hassan.hashemi@gmail.com

Mohammadhossein Salehi
salehi51280@yahoo.com

Amirreza Zare
amirreza.vs.zare@gmail.com

Narges Sadat Shourabi
narges.shourabi79@gmail.com

Saeideh Moradalizadeh
saeideh.moradalizadeh71@gmail.com

1 Department of Environmental Health Engineering, School of Health, Shiraz University of Medical Sciences, Shiraz, Iran

2 Student Research Committee, School of Health, Shiraz University of Medical Sciences, Shiraz, Iran

3 Research Center for Health Sciences, Institute of Health, Shiraz University of Medical Sciences, Shiraz, Iran

4 Environmental Health Engineering Research Center, Kerman University of Medical Sciences, Kerman, Iran

5 Department of Environmental Health Engineering, Faculty of Public Health, Kerman University of Medical Sciences, Kerman, Iran

6 Department of Chemical Engineering, School of Chemical and Petroleum Engineering, Shiraz University, Shiraz, Iran

Published online: 09 April 2024

Introduction

The health of people and other living things is threatened by the presence of heavy metal ions, radioactive pollution, pharmaceuticals, organic dyes, and other substances that are derived from human activity in aquatic environments (Rajabi et al. 2022; Hashemi et al. 2023). These pollutants disrupt the ecological equilibrium and produce secondary pollution in addition to having a direct adverse effect on individuals and the ecosystem. Consequently, preserving ecological balance, rehabilitating the ecosystem, and supplying healthy drinking water have become challenging tasks (Karimi et al. 2023; Morovati et al. 2023a; Amiri Fard et al. 2023).

Environmental, public health and safety concerns have been raised by the release of manufacturing wastes into the environment. Industrial wastewater including; tanneries, leather, petrochemicals, pharmaceuticals, and textiles puts a lot of strain on the aquatic ecology, which makes it quite dangerous. Additionally, it harms human health by impairing reproduction and causing endocrine abnormalities (Pezeshki et al. 2023; Javid et al. 2019).

Pharmaceutical and personal care products (PPCPs) have a many uses in the medical cares, commerce, farming, and etc. Due to their ubiquitous human use and inadequate removal by traditional biological treatment in water and wastewater treatment facilities, these chemicals are found everywhere in the environment (Malakootian et al. 2019a, 2019b; Zhu et al. 2022; Gharaghani et al. 2024). Numerous investigations have demonstrated that the concentration of PPCP in surface water ranges from nanograms per liter to micrograms per liter. Also, this kind of pollution has been found in subsurface water at the greatest concentrations, even reaching micrograms per liter (Malakootian et al. 2019c, 2019d; Nasiri et al. 2024).

Metronidazole (MNZ) is one of the antibiotics that are most frequently administered around the world. The antibiotic metronidazole, whose chemical formula is $C_6H_9N_3O_3$, is frequently used to cure animal and human infectious illnesses (Nasiri et al. 2019). These diseases include bacterial septicaemias, infections of the liver and intestines, amoebiasis of the liver and joints, bacterial vaginosis, and fallopian tube abscess in females, as well as infections of the lower respiratory tract and skin caused by anaerobic bacteria. MNZ is categorized as a medication that causes cancer and mutagenesis due to the damage it produces to human lymphocytes and the cytotoxic it emits, which can damage DNA, cell membranes, and proteins of living organisms considered genotoxic (Tamaddon et al. 2020; Ighalo et al. 2020; Ghiasi et al. 2022; Yurtay and Kılıç 2023).

There are several techniques for treating wastewater, including physical, chemical, and biological methods. To remove non-degradable contaminants, physical methods involve mechanical operations or filtering techniques like sedimentation and flotation. Bacteria are used to break down organic contaminants in biological processes including biologically activated sludge bioreactors, microbiological treatments, and enzymatic degradation (Mahdizadeh et al. 2020; Malakootian et al. 2020; Firoozi et al. 2023; Pourshaban-Mazandarani et al. 2023; Yazdanpanah et al. 2023). Some of the most popular chemical procedures are coagulation, chemical neutralization, adsorption, precipitation, disinfection, and ion exchange. Chemical methods employ chemicals to separate or convert contaminants. Chemical methods increase the persistent organic pollutant removal of the product and typically do not produce sludge, which results in disinfection and removes the color and smell of water. In contrast to other methods, which have drawbacks such as high initial capital and high energy costs, slow process speed, etc., chemical methods increase the biological degradation of the product (Malakootian et al. 2020a, 2020b, 2013; Nasiri et al. 2021; Fadaei et al. 2017; Hashemi et al. 2017; Rahmani et al. 2022).

Utilizing adsorption proves to be a cutting-edge and economically viable approach for treating water and wastewater in today's world, utilized to remove numerous sorts of contaminants owing to its effectiveness, simplicity, and environmental friendliness (Pourzamani et al. 2017; Chavoshani et al. 2018; Amirmahani et al. 2023). Even from diluted solutions, secondary pollutants won't be formed even if the adsorption mechanism is capable of eliminating contaminants at low concentrations. Physical and chemical adsorption are the two subcategories of adsorption (Mehdinejad et al. 2018; Pourzamani et al. 2018). When hydrogen bonds, van der Waals forces, and polar and dipole–dipole forces (which are visible between two polar molecules) are acting on both the adsorbent and the adsorbed, physical adsorption takes place. The electrostatic attraction of metal ions over the material's surface is the result of this physical process (Sadeghi et al. 2018; Mohammadi et al. 2019). Chemical bonds or electron transfer are what drive the interaction between the adsorbed substance and the adsorbent surface in the case of chemical adsorption. Active adsorption is the term used to describe this ongoing response. This matter results in the irreversibility of this class of reactions and renders chemical adsorption irreversible in contrast to its physical counterpart (Sharifi et al. 2022; Maleky et al. 2022).

The proper surface covering is crucial for boosting adsorption capacity while maintaining structural and surface stability. Organic compounds, biological molecules, polymers, surfactants, metal oxides/sulfides, metals or nonmetals, and silica are frequently used to coat surfaces (Nasiri et al. 2021). Organic or inorganic coatings can be utilized to further functionalize nanomaterials with functional groups like $–NH_2$, –SH, and –COOH. They also serve to stabilize

nanomaterials and stop them from aggregating (Malakootian et al. 2019e). Chitin stands out as the predominant biopolymer found in nature and serves as the precursor to chitosan. Its occurrence spans across various eukaryotic organisms, encompassing fungi, insects, and crustaceans. The application of chitin or chitosan in wastewater treatment is significant. Accordingly, several research investigations have demonstrated how effectively chitosan and its composites may remove contaminants from wastewater through their capacity as biosorbents. Chitosan derivatives are employed as adsorption additives in various research studies because of their outstanding capabilities (Malakootian et al. 2018a; Nasiri et al. 2022a).

This investigation introduces a pioneering magnetic nano-adsorbent, $AgZnFe_2O_4$@Ch, for MNZ removal, crafted in the presence of a Ch biopolymer, something unprecedented occurred for the first time. The advantageous aspects include the rapid, eco-friendly, and highly efficient production of this magnetic nano-adsorbent with Ch as a biopolymer, free from harmful solvents and surfactants. Consequently, a greater deposition of MNZ molecules on the $AgZnFe_2O_4$@Ch surface occurs, fostering increased contact and thereby enhancing adsorption. Alongside optimizing factors like solution pH, MNZ starting concentration, contact duration, and adsorbent dose, the study also delves into adsorption isotherms, thermodynamics, and kinetics. Chemical stability and reusability of the nanoadsorbent were additionally assessed.

Materials and methods

Chemicals and instrumentation

Zinc (II) chloride ($ZnCl_2$), iron (III) chloride hexahydrate ($FeCl_3.6H_2O$), silver chloride (AgCl), hydrogen chloride (HCl), sodium hydroxide (NaOH), and chitosan (Ch) were provided by Sigma Aldrich and Merck, while metronidazole was bought from Amin Darou Pharmaceutical Manufacturing Company (Isfahan, IRAN). Deionized water was utilized to produce all of the experiment's aqueous components. After adjusting pH using 1 *N* solutions of HCl and NaOH, the outcome was gauged using a pH measurement device (HANNA instruments, model pH 212). The determination of MNZ concentration was performed utilizing a UV–visible spectrophotometer (DR 5000) operating at optimal wavelengths of 321 nm. With the use of XRD, EDS-Mapping, TGA, FTIR, BET, VSM, and FESEM, the nanoadsorbent structure was examined. To examine the structural characteristics and composition of the magnetic nano-crystal adsorbent, XRD (PHILIPS PW1730) and FESEM (TESCAN MIRA III) were employed. Additionally, EDS-mapping (TESCAN MIRA II, SAMX Detector) was utilized to ascertain the types, weight percentages, and distributions of elements on the surface of the magnetic nanoadsorbent. Moreover, BET assessment was employed to determine the specific surface area of the magnetic nanomaterial (BELSORP MINI II), FTIR spectroscopy was applied to examine the chemical bonds within the magnetic nano-adsorbent and identify its functional groups (AVATAR, Thermo), and the magnetic properties of the magnetic nano-adsorbent (LBKFB, Kashan Kavir Magnet Company) were evaluated using VSM. The degradation of MNZ from an aqueous media was carried out employing the magnetic nanoadsorbent after its chemical and physical characteristics had been established.

Synthesis of $AgZnFe_2O_4$@Ch

Prior to dissolving the $FeCl_3.6H_2O$ and $ZnCl_2$ salts in 100 mL of distilled water at 80 °C and sonicating for 30 min, the salts $FeCl_3.6H_2O$, $ZnCl_2$, and AgCl were first weighed in a ratio of 1:0.5:0.5. At a temperature of 80 °C, 50 mL of ammonia (NH_3) was mixed with AgCl, and the mixture was then sonicated for 30 min. After that, the mixture liquid was kept at 80 °C, and 1 g of chitosan (Ch) was added. Chitosan was completely dissolved, and the mixture was then given one more stir while being put on a heated plate for over a day at a temperature of 30 °C, along with 5 g of NaOH and the silver chloride solution. The concentrated solution obtained is subjected to drying in an oven at 110 °C, followed by multiple rinsed using distilled water until achieving a neutral pH, then dried once more as a black powder for 24 h as a nanoadsorbent at 70 °C (Naghizadeh et al. 2021).

Adsorption experiments

As variables affecting the adsorption process, pH, adsorbent dose, starting MNZ concentration, contact period, and temperature were all evaluated and changed. From a 500 mg/L stock MNZ solution, antibiotic concentrations of 5, 10, 15, 20, and 30 mg/L were developed. To maximize the dose of the adsorbent, the doses of 0.3, 0.6, 0.9, 1.2, and 1.5 g/L were utilized. The study examined contact times of 10, 20, 30, 40, 50, and 60 min, temperatures of 25, 30, 35, and 40 °C, and pH ranges of 3, 5, 7, 9, and 11. The subsequent equations were applied for the computation of the adsorbent's adsorption capacity (Eq. 1) and the MNZ adsorption performance (Eq. 2):

$$Q = \frac{(C_0 - C_t)\,V}{M} \tag{1}$$

$$\text{Removal Efficiency}\,(\%) = \frac{C_0 - C_t}{C_0} \times 100 \tag{2}$$

The values of C_0 and C_t (mg/L) reflect the concentrations of MNZ before and after the contact period, correspondingly.

Q stands for adsorption capacity (mg/g), V for volume of sample (L), and M for adsorbent dose (g/L) (Nasiri et al. 2022a, 2022b).

Determine the pH point of zero charge (pH_{pzc})

50 mL of a KCl 0.1 M solution was used for evaluating pH_{pzc} along with 0.01 g of magnetic nanoparticles in six distinct pH ranges (2, 4, 6, 8, 10, and 12). The solutions were prepared, and their ultimate pH was assessed after being shaken for 24 h. A curve illustrating the pH change was produced using the variables X = initial pH and Y = pH. The X-axis's intersection with the curve is represented by the value of pH_{pzc} (Nasiri et al. 2022c; Morovati et al. 2023b).

Modeling and optimization using design-expert

Design-Expert is a statistical software package widely used for designing experiments and analyzing experimental data. The modeling part of Design-Expert involves creating mathematical models to represent the relationships between input factors and the response variable in an experimental design. Users can employ techniques like regression analysis and factorial designs to create models that represent the impact of individual factors and their interactions on the response. The software facilitates the exploration of various model configurations, enabling users to identify and focus on the most influential factors affecting the outcomes of interest. Through the modeling process, researchers can gain insights into the underlying dynamics of their experiments and make informed decisions about optimal factor settings. Design-Expert provides graphical tools, such as contour plots and 3D surface plots, to visualize response surfaces and aid in interpretation (Estahbanati et al. 2017). The software's user-friendly interface makes it accessible for scientists and engineers to conduct robust experiments and enhance the understanding of their processes. In this research, data design and analysis were conducted using the Design-Expert 13 software (Yakoubi et al. 2021). Table 1 lists the variety of factors that were examined. The Table 1 provides information on the independent factors considered in the study related to MNZ adsorption. Each factor includes units of measurement, coded values, the mean square, and standard deviation. The factors include Adsorbent concentration (A), MNZ concentration (B), pH (C), temperature (D), and time (E), each with specific ranges denoted by coded low and high values, providing insights into the experimental design and conditions explored in the study.

Results and discussion

Specification and characterization of $AgZnFe_2O_4$@Ch

The FTIR spectra of Ch and $AgZnFe_2O_4$@Ch were compared to the KBr pellet in so as to determine the groupings that function in the produced nanoparticles (Fig. 1). FTIR spectra were employed to identify the matching bands for the Ch vibration absorption. O–H stretch takes place at 3419 cm^{-1}, while C–H stretching was at 2921 and 2861 cm^{-1}. NH primary amine bends manifested at 1620 cm^{-1}, C–O in the primary alcoholic group exhibited vibrations at 1381 cm^{-1}, and C–O–C bridge displayed asymmetric movements at 1158 cm^{-1}. Additionally, C–O stretching was detected at 1065 and 1030 cm^{-1}, the $–NH_2$ free amino group resonated at 1026 cm^{-1}, and C–N stretching occurred at 865 cm^{-1} (Carvalho et al. 2010; Fernandes Queiroz et al. 2015; Wiercigroch et al. 2017; Oliveira et al. 2015; Sekiguchi et al. 2003). The $AgZnFe_2O_4$@Ch nano-adsorbent was found to include the following vibration absorption bands, according to FTIR spectra. The presence of Ch in the nano-adsorbent configuration is evidenced by specific bands occurring at 1631 cm^{-1}, representing –NH primary amine bending, 1388 cm^{-1}, indicating the presence of the C–O in the primary alcoholic group, and 1031 cm^{-1}, signifying the $–NH_2$ free amino group. Additionally, the metal spinel ferrite structure's confirmation involves two distinctive absorption peaks observed at 591 and 467 cm^{-1}, respectively. These peaks showed the presence of the intrinsic stretching vibrations of the metal cation at the tetrahedral site M_{tetra}–O and the metal cation at the octahedral site M_{octa}–O, which were linked to the distinctive peak of $AgZnFe_2O_4$@Ch (El-Sayed 2002; Mallapur et al. 2009; Varma and Vasudevan 2020).

To evaluate the shape, morphology, and dimensions of the synthesized $AgZnFe_2O_4$@Ch, FESEM images were employed (Fig. 2 a–c). Chitosan causes the $AgZnFe_2O_4$@Ch structure to produce a sphere-shaped, uniformly

Table 1 Independent factors on MNZ adsorption

Factor	Name	Units	Coded low	Coded high	Mean	Std. dev
A	Adsorbent	g/L	−1 ↔ 0.30	+1 ↔ 1.50	0.8806	0.2786
B	MNZ concentration	mg/L	−1 ↔ 5.00	+1 ↔ 30.00	8.55	5.35
C	pH	–	−1 ↔ 3.00	+1 ↔ 11.00	7.00	1.15
D	Temperature	Celsius	−1 ↔ 25.00	+1 ↔ 40.00	25.97	3.27
E	Time	Minute	−1 ↔ 10.00	+1 ↔ 60.00	50.00	6.32

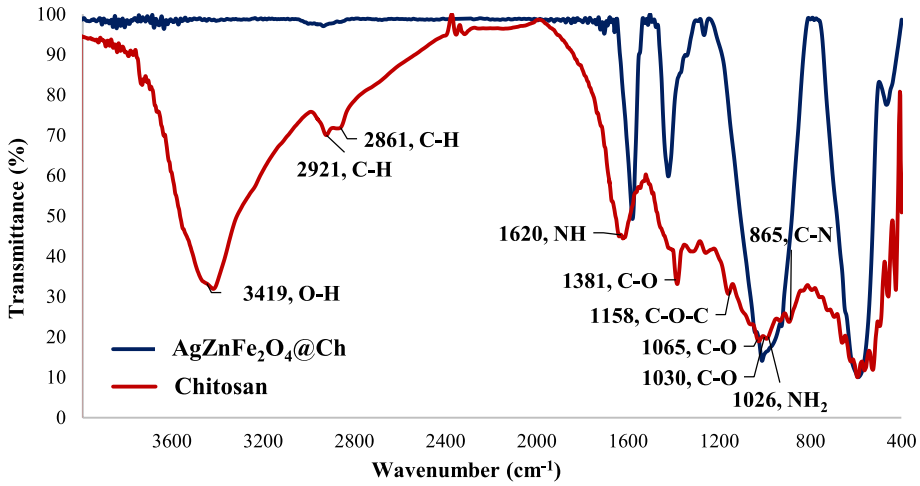

Fig. 1 FTIR of chitosan and $AgZnFe_2O_4$@Ch magnetic nanoadsorbent

dispersed, and slightly aggregated magnetic nano-heterogeneous catalyst. In Fig. 2d, the particle size distribution is displayed. The graph depicting the dispersion of particle sizes indicates that the average size of $AgZnFe_2O_4$@Ch particles falls within the range of 50 to 100 nm.

To ascertain the phases, structure, and crystal composition of $AgZnFe_2O_4$@Ch, XRD analysis was used. Figure 3 shows all of the results. Following the Joint Committee on Powder Diffraction Standards (JCPDS 96–591-0064), the crystal phase structure and XRD pattern of $AgZnFe_2O_4$@Ch reveal diffraction peaks at $2\theta = 30.06°$, 35.36°, 38.25°, 42.96°, 44.42°, 53.22°, 56.75°, 62.31°, 64.62°, 73.93°, and 77.55°, indicating the cubic spinel phase of $AgZnFe_2O_4$. Additionally, a weak peak at $2\theta = 18.34°$ is observed, associated with the chitosan structure, albeit with decreased intensity in the final nanoadsorbent structure (Liu et al. 2021; Malakootian et al. 2019f). In that final nanoadsorbent construction the Ch peak's strength has been lessened but not entirely eliminated. The contribution of Ch to the reaction during the adsorbent's production has resulted in a drop in Ch's peak intensity. The findings demonstrate that in the Ch-containing composition, the $AgZnFe_2O_4$ crystal structure was successfully preserved. The Debye–Scherrer equation (Eq. (3)) was utilized to determine the average crystalline size of $AgZnFe_2O_4$@Ch, in which the determined value was 32.7 nm. The variables λ, θ, and β represent the X-ray wavelength, the Bragg angle, and the line broadening at the full-width at half maximum (FWHM) of the most intense peak, respectively (Malakootian et al. 2019g).

$$D = \frac{0.9\lambda}{\beta \cos\theta} \tag{3}$$

EDS assessment was utilized to evaluated the chemical makeup and purity of the generated $AgZnFe_2O_4$@Ch (Fig. 4a). With regard to the EDS outcomes, the $AgZnFe_2O_4$@Ch magnetic nanoadsorbent has amounts of 10.16% Ag, 7.47% Zn, 25.19% Fe, 26.18% O, 6.66% N, and 24.33% C that are all within the range that was expected. A precise component distribution analysis is required for the study of mapping. The $AgZnFe_2O_4$@Ch elements' dispersion was studied using it. As illustrated in Fig. 4b, the homogeneous distribution of Ag, Zn, Fe, O, N, and C demonstrated the great homogeneity of the synthesized $AgZnFe_2O_4$@Ch.

The BET-Plot and adsorption/desorption isotherm of $AgZnFe_2O_4$@Ch are shown in Figs. 5a–d, respectively. The assessment of the BET surface area for the $AgZnFe_2O_4$@Ch nanocomposite involved N_2 adsorption/desorption analyzes. The BET equation was applied for the calculation of the monolayer gas adsorbed volume, enabling the inference of the catalyst's surface area (Rajabi et al. 2022). The BET plot was utilized to compute various parameters for the synthesized magnetic nanoadsorbent, including the total pore volume ($p/p_0 = 0.990$), specific surface area (19.246 m^2/g), and mean pore diameter (27.837 nm). According to the degree of contact between the adsorptive surface and the sample surface and whether or not pores are present, adsorption isotherms are divided into different categories. The categorization of adsorption isotherms, according to the International Union of Pure and Applied Chemistry (IUPAC), involves the classification of pores into mesoporous, macroporous, or microporous based on their diameter. Mesoporous materials, as per IUPAC, exhibit pores within the size range of 2–50 nm, while macroporous pores exceed 50 nm in diameter, and microporous pores have diameters below 2 nm. The image portrays a Type-IV isotherm with a noticeable hysteresis loop between the desorption and adsorption branches is shown in the image for the mesoporous material $AgZnFe_2O_4$@Ch (Nasiri et al. 2022b).

Figure 6 shows the findings for the saturation magnetization (Ms), coercive force (Hc), and residual magnetization

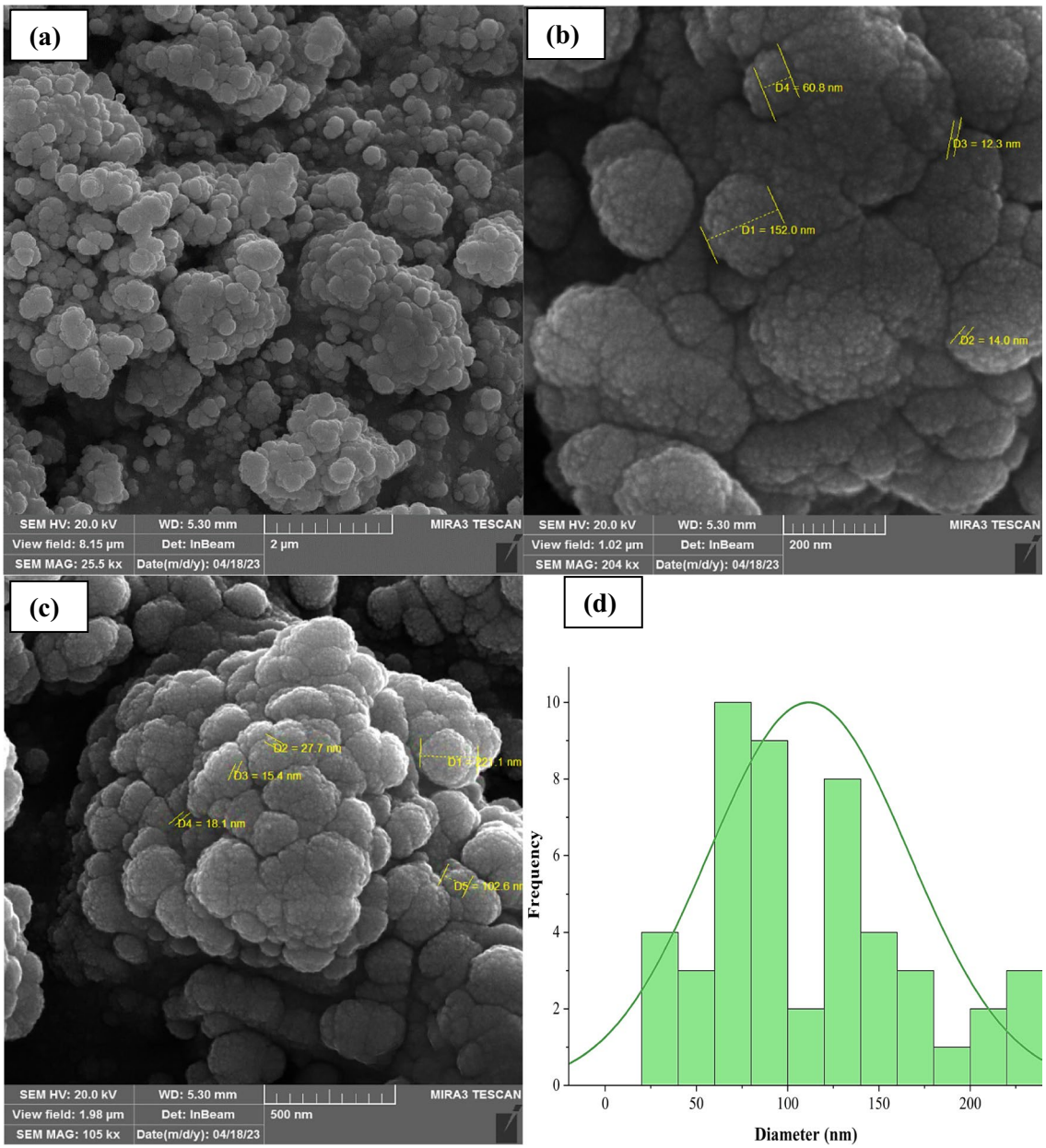

Fig. 2 FESEM images (**a**–**c**) of $AgZnFe_2O_4$@Ch magnetic nanoadsorbent and size distribution (**d**)

(Mr) of $AgZnFe_2O_4$@Ch, which were 14.64 emu/g, 50 Oe, and 1.12 emu/g, correspondingly. These observations suggest the notable magnetic properties of $AgZnFe_2O_4$@Ch. With the use of an external magnet, the $AgZnFe_2O_4$@Ch magnetic nanoadsorbent may be quickly removed throughout the periods of regeneration and reuse, from the reaction media. This is made possible by the adsorbent's high magnetic properties.

Conducting the TGA of $AgZnFe_2O_4$@Ch involved subjecting it to an N_2 atmosphere, with temperatures altering from ambient to 500 °C (increasing at a rate of 20 °C min^{-1}). The objective was to emphasize the significance of adsorbent thermal stability in various industrial utilization. The thermal degradation of $AgZnFe_2O_4$@Ch manifested in a tripartite manner (Fig. 7). The initial phase of mass reduction occurs within the temperature altering of 20 to 100 °C, attributed to the loss of absorbed water. The subsequent stage involves the breakdown of the majority of Ch, initiating at 100 °C and peaking at a maximum rate around 410 °C. The disintegration of polysaccharide chains, vaporization, and elimination of breakdown by products such as deamination, dehydration, disruption of glycoside structures, deacetylation, and ring-opening of pyranose is responsible for the 1.263% mass loss at this step (Nasiri et al. 2022a). There was no discernible effect

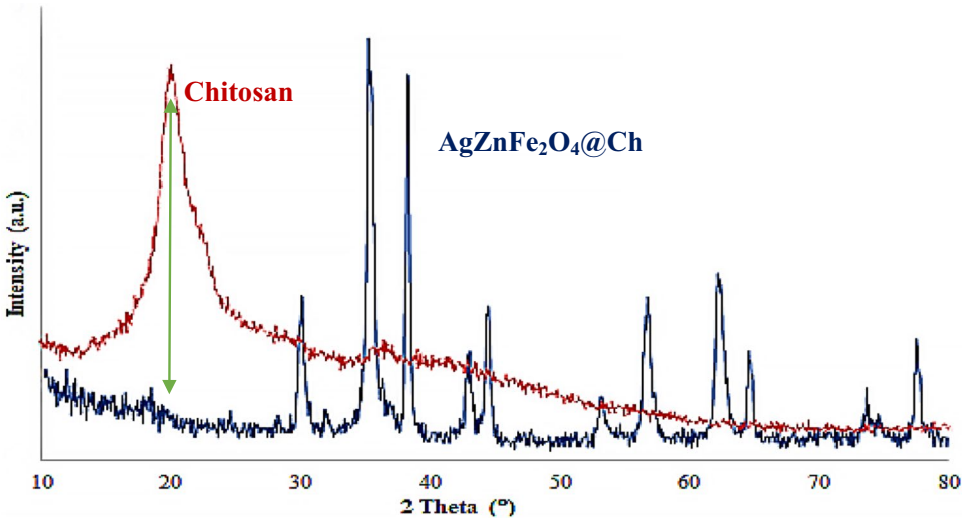

Fig. 3 XRD pattern of $AgZnFe_2O_4$@Ch magnetic nanoadsorbent

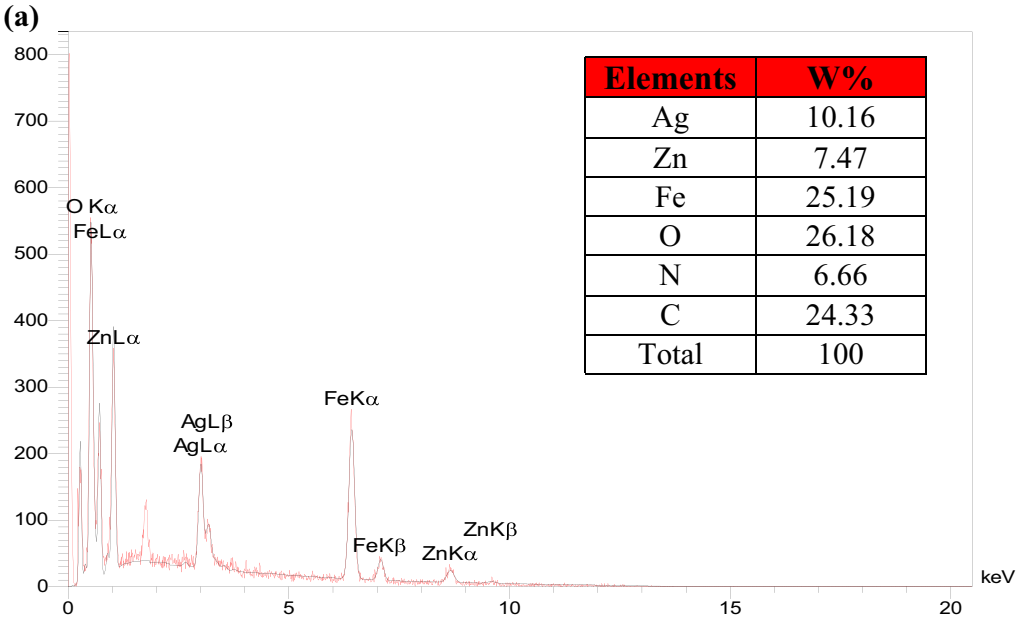

Elements	W%
Ag	10.16
Zn	7.47
Fe	25.19
O	26.18
N	6.66
C	24.33
Total	100

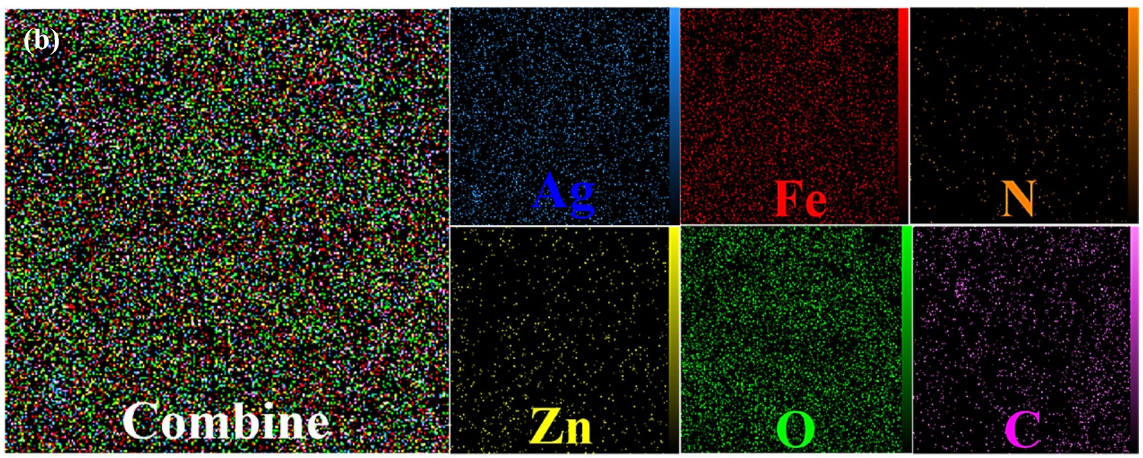

Fig. 4 EDS and mapping of $AgZnFe_2O_4$@Ch magnetic nanoadsorbent

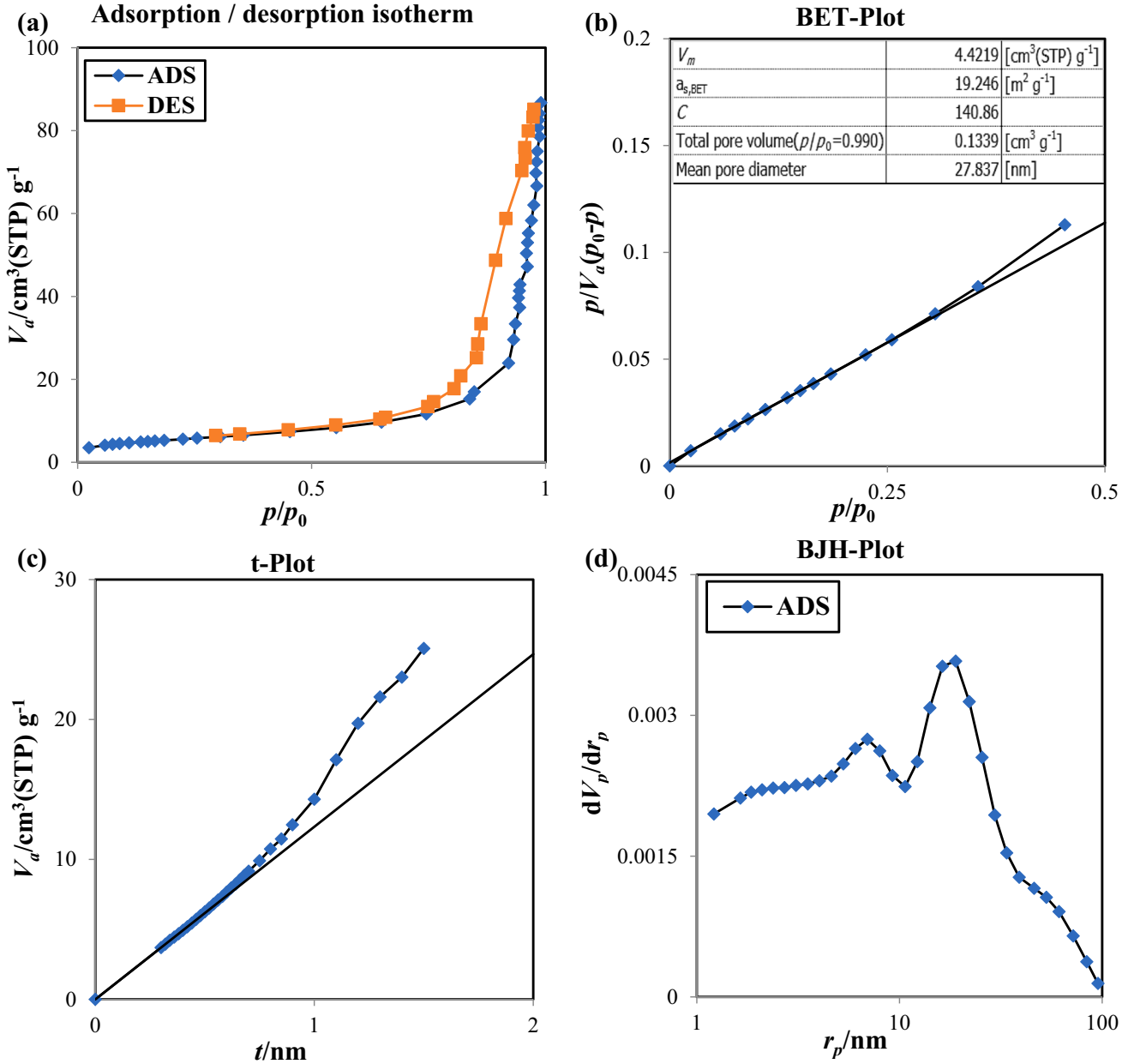

Fig. 5 Adsorption/desorption isotherm (**a**), BET surface area (**b**), t-Plot (**c**), and BJH-Plot (**d**) of $AgZnFe_2O_4$@Ch nanoadsorbent

of the third stage, which ran from 410 to 500 °C, on weight reduction. According to the figure, at 500 °C, the adsorbent lost 1.589% (0.074 mg) of its weight. This finding demonstrates $AgZnFe_2O_4$@Ch's thermal stability.

Optimization of effective parameters on MNZ adsorption

Effect of adsorbent dose

Figure 8 depicts how the quantity of the nanoadsorbent affects the efficiency of MNZ removal after 60 min. In this procedure, the starting MNZ concentration was 5 mg/L, the initial volume of the solution was 100 mL, and multiple dosages of nanoadsorbents (0.3, 0.6, 0.9, 1.2, and 1.5 g/L) were evaluated. By using more nanoadsorbent from 0.3 to 0.9 g/L, the MNZ adsorption efficiency was improved from 51.7 to 68% after 50 min. The removal efficacy increased by 77.5% at higher nano sorbent doses of 1.5 g/L, but because this improvement in removal efficiency was not noticeable and was not financially advantageous, the optimum dosage of 0.9 g/L nanoadsorbent with 68% elimination effectiveness was decided to take into consideration. The increased adsorbent dose may result in greater removal efficiency due to the adsorbent's expanded surface area and the

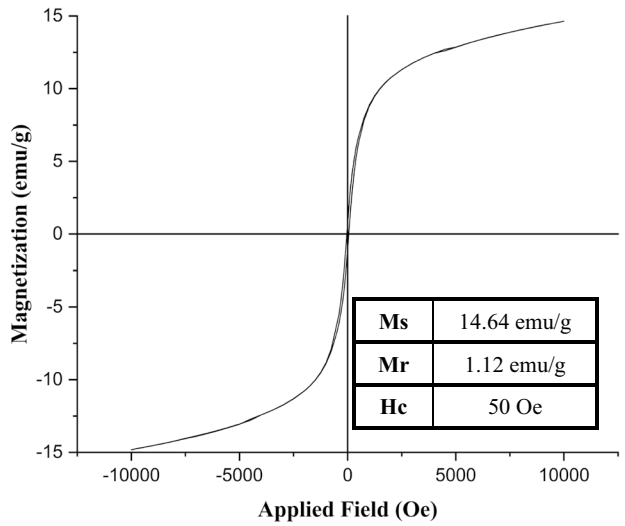

Fig. 6 VSM magnetization curve of $AgZnFe_2O_4$@Ch magnetic nanoadsorbent

extra adsorption sites availability. Nevertheless, because the concentration of MNZ remained constant and there was little to no increase in the amount of interaction between the antibiotic molecules and the adsorbent nanoparticles, its adsorption rate did not significantly rise with increasing adsorbent dose. Nasseh et al. (2019) investigated MNZ adsorption in the same investigation. They concluded that the degradation effectiveness of metronidazole rises with an improvement in adsorbent quantity.

Effect of pH

One important factor that significantly influences the adsorption performance is the pH of the aqueous media. The binding of pollutants onto the adsorbent during this process typically results from the functional groups, surface charges, degree of ionization, and saturation of the adsorbent. The effects of pH on the adsorption efficiency of MNZ by magnetic nanoadsorbent are shown in a time frame of 10 to 60 min (Fig. 9a), assuming that the starting concentration of MNZ was 10 mg/L and the optimal quantity of nanosorbent (0.9 g/L). Although there was not much of a difference in the adsorption efficiency between pH 5 and 7 and since the highest removal efficiency was at pH 5, which was 67.5%, and subsequently declined to 27.3% at pH 11 at 50 min, it was determined that pH 7 was the ideal pH. The efficacy of the adsorption procedure, however, is also affected by the adsorbent pH_{pzc}. The pH_{pzc} of $AgZnFe_2O_4$@Ch nanoadsorbent was evaluated like this and was found to be 6.4 (Fig. 9b). It was discovered that the adsorbent surface is positive at pHs under 6.4 and negative at pHs over 6.4 based on the pH_{pzc} value for the nano sorbent. With an acid dissociation constant (pKa) of 2.55, MNZ may exist in several kinds of ionic forms at different pH values. MNZ molecules could be observed in anionic form above pH 2.55, whereas cationic form may be found below pH 2.55 (Nasiri et al. 2022b). Since the MNZ molecule is present in anionic form and the adsorbent surface has a positive charge, the optimal pH for this approach was reported to be 7. This indicates that at this pH, the presence of electrostatic attraction forces may exert a notable influence on the adsorption procedure of contaminants onto the surface of the adsorbent. Moreover, given that MNZ is an organic compound within the aqueous environment, it has a tendency to separate from the solution due to the influence of lyophobic interactions, approaching the adsorbent surface in such circumstances (Malakootian et al. 2019d). Aarab et al. (2020) evaluated the adsorption of MNZ. They assessed that metronidazole

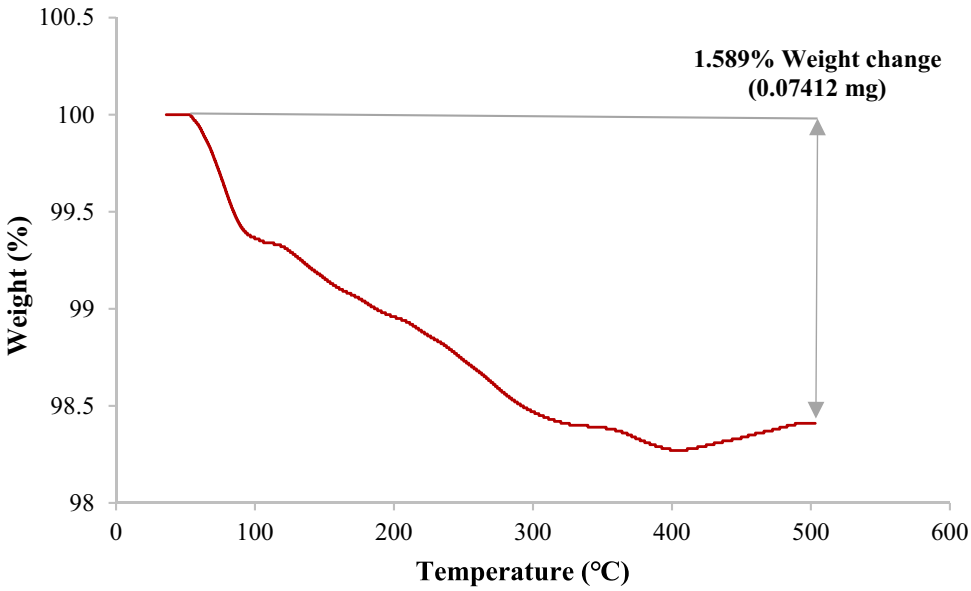

Fig. 7 TGA pattern of $AgZnFe_2O_4$@Ch magnetic nanoadsorbent

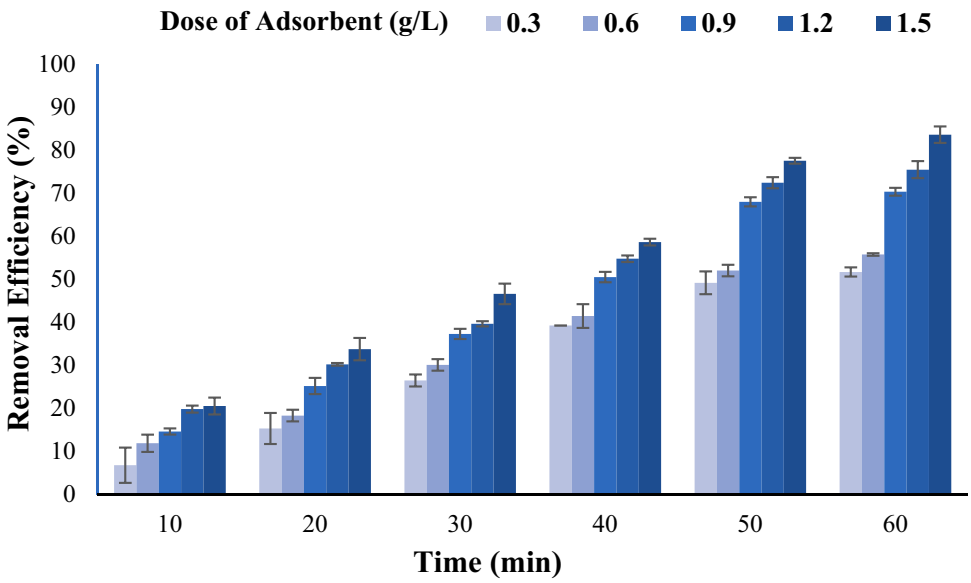

Fig. 8 Effect of various adsorbent dose (g/L) (MNZ concentration 5 mg/L, temperature 25 °C, pH 7)

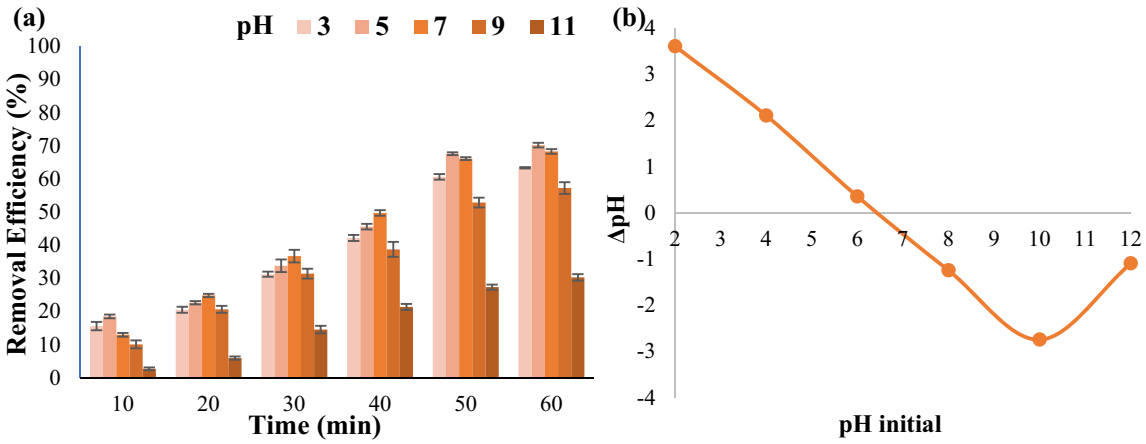

Fig. 9 Effect of various pHs (**a**) and the zero point of charge (pH_{zpc}) (**b**) (MNZ concentration 10 mg/L, temperature 25 °C, dose of adsorbent 0.9 g/L)

removal effectiveness decreases as pH increases, with acidic pHs exhibiting the highest removal effectiveness.

Effect of MNZ concentration

To investigate the effects of changes in MNZ concentration on its removal efficacy, MNZ solutions at concentrations of 5, 10, 15, 20, and 30 mg/L were in contact with 0.9 g/L of $AgZnFe_2O_4$@Ch magnetic nanoadsorbent at a temperature of 25 °C and an ideal pH of 7 (Fig. 10). The optimal level of MNZ in the process was 10 mg/L, since, based on the results of concentration variations, the adsorption effectiveness of MNZ decreased from 68.3 to 40.8% as the first concentration of MNZ solution increased, progressing from 5 to 30 mg/L, and given that the rate of adsorption in the concentration of 10 was not substantially reduced with the concentration of 5. While the density of MNZ molecules in the solution increases with initial concentration, the sites that are active on the adsorbent surface become saturated promptly and the efficiency of MNZ removal decreases (Nasseh et al. 2019). Tetracycline removal research by Guo et al. (2016) found that when the concentration of the drug rose, the effectiveness of its removal dropped.

Effect of temperature

The temperature has an influence on the adsorption performance as well. Figure 11 shows how temperature changes affect the effectiveness of metronidazole's adsorption. The examination into the impacts of process temperature (25, 30, 35, and 40 °C) on the removal effectiveness of MNZ by magnetic nanoadsorbent found that at 25 °C temperature,

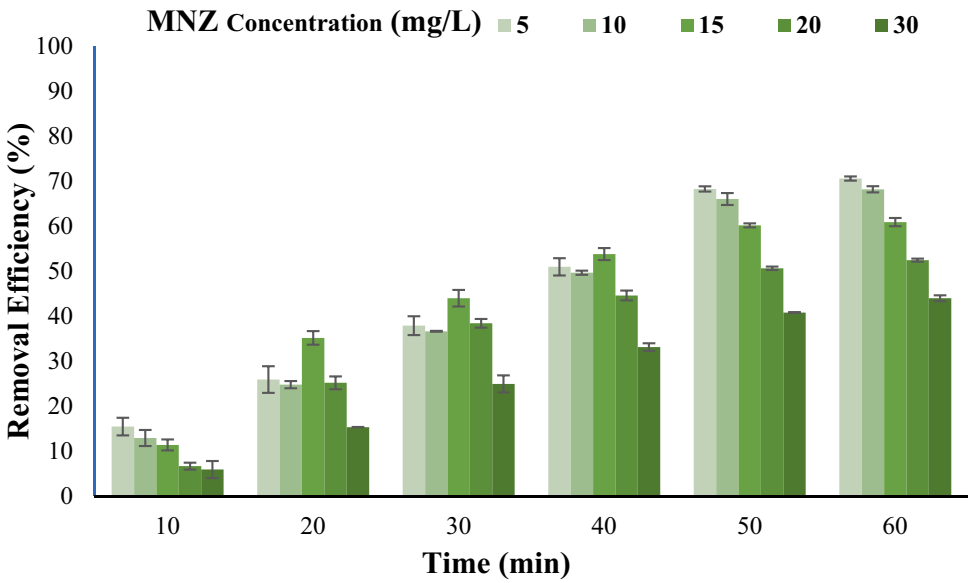

Fig. 10 Influence of different MNZ concentration (mg/L) (dose of adsorbent 0.9 g/L, temperature 25 °C, pH 7)

66.5% of the antibiotic was efficiently adsorbable at a concentration of 10 mg/L of MNZ and pH 7. The efficiency of MNZ removal declined to 58.2% at 40 °C, attributed to a decline in the removal rate with the rise in temperature to that level. This result illustrates both physical adsorption and the exothermic character of the adsorption process. Exothermic processes go in the opposite direction when the temperature rises. Temperature rise causes a reduction in physisorption. This results from adsorption's exothermic nature, which causes previously attached particles to be ejected at higher temperatures when their weak Van Der Waal bonds disintegrate. The system will attempt to dissipate heat by altering the equilibrium in favor of the endothermic direction, which is typically the direction of desorption if the temperature rises. As a result, the absorbent will release more absorbates, decreasing the effectiveness of adsorption (Malakootian et al. 2019d). Aarab et al. (Aarab et al. 2020) researched MNZ adsorption as temperature increased. The highest absorption of MNZ happens at room temperature, and the efficacy of MNZ elimination reduces with increasing temperature, regarding to the study.

Kinetics study of MNZ adsorption

Understanding reaction rates and how they are affected by various factors is made easier by kinetics. Additionally, defining the properties of a chemical reaction and gathering

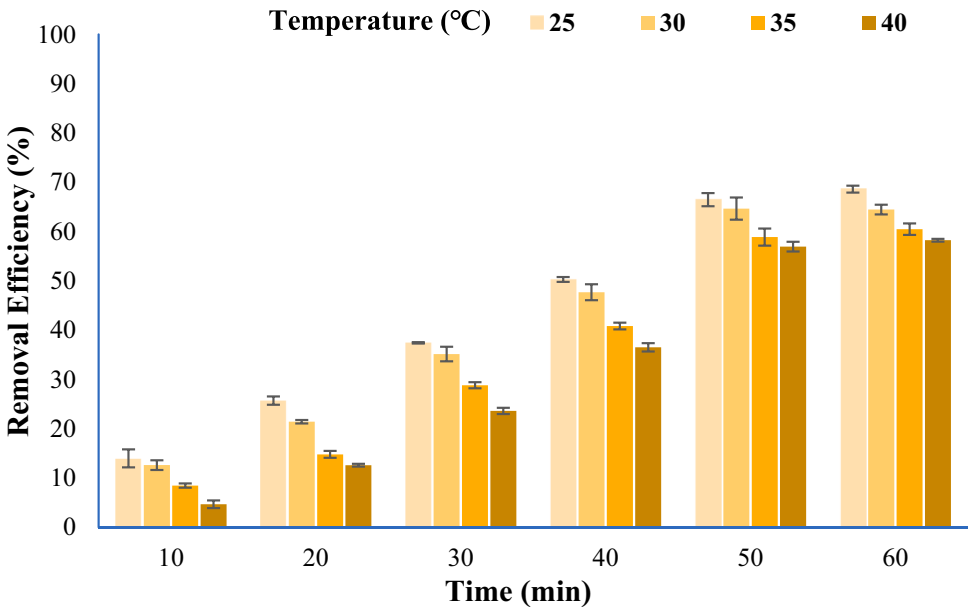

Fig. 11 Effect of various temperatures (MNZ concentration 10 mg/L, pH 7, dose of adsorbent 0.9 g/L)

and analyzing data on the reaction's process is helpful. *Pseudo*-first-order (Eq. 4) and *pseudo*-second-order (Eq. 5) classical models can be utilized to describe surface adsorption kinetics. These two models are used in a broad array of adsorption systems, such as the pollutions adsorption comprising heavy metals and pharmaceuticals, as well as biomass and nanomaterials as an adsorbent. Among adsorption kinetics models, intraparticle diffusion kinetics (Eq. 6) models are frequently employed. This kinetics study investigates adsorption on the active constituents of the adsorbent, internal diffusion or intraparticle diffusion to transport the adsorbent in the pores in the adsorbent, and exterior diffusion or film diffusion to transport the adsorbent in the liquid film around the adsorber. With the use of the following equations, these kinetics models were investigated:

$$\log\left(q_e - q_t\right) = \log q_e - K_1 t \tag{4}$$

$$\frac{t}{q_t} = \frac{1}{K_2 q_e^2} + \frac{1}{q_e} t \tag{5}$$

$$q_t = k_i t^{0.5} + C \tag{6}$$

K_1 represents the rate constant for adsorption in the pseudo-first-order model (1/min), along with the time of adsorption (t), and q_t and q_e indicating the quantity of adsorbate on the adsorbent (mg/g) at initial and equilibrium times. The determination of the R^2 coefficient and the amount of the K_1 constant involved the construction of a graph depicting log (q_e–q_t) against time (t). The speed parameters were determined by plotting t/q_t versus t on a graph. To get the amounts of K_2 and q_e, the y-intercept and slope of the plot were utilized (Nasiri et al. 2022c). The magnitude of the intercept directly correlates with the prominence of the influence of surface adsorption during the level-limiting phase, where C denotes the boundary layer effect or surface adsorption, and k_i denotes the intraparticle diffusion rate constant (g/mg min) (Nasiri et al. 2022b).

The results of the kinetic analyzes of the $AgZnFe_2O_4$@Ch-mediated MNZ adsorption process are presented in Table 2. Since the value of R^2 in the intraparticle kinetic model ($R^2 = 0.996$) is higher than the value of R^2 in the other models, it is utilized to describe the adsorption performance. As a result, MNZ efficiently adsorbed utilizing an intraparticle kinetic model on the magnetic nanoadsorbent $AgZnFe_2O_4$@Ch. According to Flores-Cano et al. (Flores-Cano et al. 2016) 's kinetic analysis, the adsorption of MNZ onto coffee-activated carbon followed the intraparticle diffusion kinetic model, which is consistent with the results of this experiment.

Isotherm study of MNZ adsorption

There are several categories under which the adsorption isotherm may be subdivided. Langmuir (Eq. 7, 8), Freundlich (Eq. 9), and Temkin (Eq. 10, 11) are among the widely favored choices for describing adsorption isotherms. The following equations were used to evaluate these isotherms:

$$\frac{C_e}{Q_e} = \frac{1}{Q_{\max} K_L} + \frac{C_e}{Q_{\max}} \tag{7}$$

$$R_L = \frac{1}{(1 + K_L C_0)} \tag{8}$$

$$\ln Q_e = \left(\frac{1}{n}\right) \ln C_e + \ln K_f \tag{9}$$

$$Q_e = B_T \ln K_T + B_T \ln C_e \tag{10}$$

$$b_T = (\mathrm{RT})/\left(B_T\right) \tag{11}$$

The started concentration of MNZ is C_0 (mg/L), C_e depicts the MNZ stability in concentration (mg/L), and $Q_{\max}$ (mg/g) is the maximal adsorption in the solid phase. The Freundlich constant presented by K_f (mg/g).(L/mg)$^{1/n}$ is the opposite of K_L, which is the Langmuir adsorption equilibrium constant (L/mg). Constant n stands for the adsorption rate (Nasiri et al. 2022b). The basic characteristics of the Langmuir isotherm may be explained using the equilibrium parameter or separation factor R_L, which predicts the suitability or unsuitability of the adsorption mechanism under study. Equation 7 was employed to specify it. R_L's value shows whether adsorption is unfavorable ($R_L > 1$), linear ($R_L = 1$), favorable ($0 < R_L < 1$), or irreversible ($R_L = 0$). The B_T and b_T are constants, while the K_T stands for the Temkin adsorption potential (L/g). The universal gas constant is denoted by R, while the temperature is denoted by T (44).

The findings from the Freundlich, Langmuir, and Temkin equilibrium isotherms are depicted in Table 3. The outcomes

Table 2 Parameters corresponding to the models for adsorption kinetics (adsorbent: 0.9 g/L, MNZ: 10 mg/L, temperature: 25 ℃, and pH: 7)

Pseudo-first-order kinetic model			Pseudo-second-order kinetic model			Intraparticle kinetic model		
R^2	K_1 (1/min)	q_e (mg/g)	R^2	K_2 (g/mg min)	q_e (mg/g)	R^2	K_P (mg/g min^{-5})	C (mg/g)
s	−0.048	0.732	0.965	2.843	0.792	0.997	0.123	0.253

suggest that the R^2 value of the Langmuir model was greater than that of the Freundlich and Temkin models ($R^2 = 0.997$ vs. $R^2 = 0.953$ and 0.982). Thus, the adsorption performance is described by the Langmuir isotherm model in a better manner. Furthermore, the Langmuir model's R_L value, which ranges from 0 to 1, indicates that adsorption is favorable. These findings are consistent with Ahmed and Theydan's isotherm investigation for the adsorption of MNZ from aqueous solutions by activated carbon of *Siri*'s seed pods, which depicted that the adsorption procedure of MNZ adopts the Langmuir isotherm (Ahmed and Theydan 2013).

Thermodynamic study of MNZ adsorption

The study of temperature in association with energy, entropy, enthalpy, and the physical characteristics of matter and radiation is known as thermodynamics. According to the following equations (Eq. 12 and 13), this study studied the thermodynamics of the MNZ adsorption process:

$$\Delta G = -RT \ln k_d \tag{12}$$

$$\ln K_d = \frac{\Delta S}{R} - \frac{\Delta H}{RT} \tag{13}$$

ΔG symbolizes changes in Gibbs free energy, where R stands for the universal gas constant with an amount of 8.314 J/mol/K. Temperature is denoted by T in K, standard entropy is represented by ΔS (kJ/mol), K_d signifies thermodynamic equilibrium, and standard enthalpy variation are implied by ΔH (kJ/mol). The determination of ΔS and ΔH involved the calculation of their values using the $\ln K_d$ vs $1/T$ graph, considering the slope and origin-intercept. This was done after calculating the thermodynamic equilibrium constant for ΔG at different temperatures (Hashemzadeh et al. 2023; Malakootian et al. 2018b).

The outcomes of thermodynamic analyzes of the MNZ adsorption procedure on the $AgZnFe_2O_4$@Ch are presented in Table 4. The results are consistent with Bouraie and Ibrahim's research on the non-spontaneous adsorption of the MNZ antibiotic using MgO (Bouraie and Ibrahim 2021), which found that the adsorption procedure is non-spontaneous. The absence of the expected enthalpy shifts demonstrates the exothermic characteristic inherent in the adsorption procedure. Additionally, the decreased disturbance in the adsorption procedure is shown by the negative standard entropy variations.

Design-expert optimization

The modified Linear model's ANOVA findings in Table 5 showed that the model could be utilized to effectively represent the MNZ removal under a variety of operational situations. Considering p-values (0.0003) were less than 0.05, the information presented in this table indicates the statistical significance of the linear model at a confidence level of 5%. The variance of the information around the fitted model is described by the likelihood of lack of fit (PLOF). A measure of the model's appropriateness in capturing the data, the determination coefficient (R^2), was somewhat substantial at the level of 58%. The accuracy in acquiring the signal-to-noise ratio is adequately ensured. It is preferable to have a ratio of at least 4. The ratio of 9.0384 in this instance denotes a sufficient signal. The low coefficient of variation values (C.V. = 14.88%) pointed to the experimental data's extremely high degree of accuracy and substantial dependability (Shahrezaei et al. 2012).

The findings of a statistical analysis of variance on the experimental data for MNZ adsorption are displayed in Table 6. The Linear model's ANOVA reveals that it is extremely significant. The model is implied to be significant by the Model F-value of 6.97. An F-value this big occurring due to noise has a 0.03% probability of happening. Model terms are considered significant if their p-values are less

Table 4 The thermodynamic parameters of MNZ adsorption (pH: 7, adsorbent: 0.9 g/L, MNZ initial concentration: 10 mg/L)

T (k)	ΔG (kJ/mol)	ΔH (kJ/mol)	ΔS (j/mol k)
298	0.674	− 0.915	− 5.331
308	0.701		
318	0.727		
328	0.754		

Table 3 Langmuir, Freundlich, and Temkin isotherm elements (adsorbent: 0.9 g/L, contact time: 50 min, pH: 7, MNZ concentration: 10 mg/L, and temperature: 25 ℃)

Langmuir				Freundlich			Temkin		
R^2	R_L	Q_{max} (mg/g)	K_L	R^2	K_F	1/n	R^2	B_1	K_T (L/mg)
0.997	0.478	1.691	0.219	0.953	2.704	0.484	0.982	0.379	2.037
	0.314								
	0.238								
	0.186								
	0.132								

Table 5 Fit summary of MNZ adsorption efficiency

Source	Sequential *p*-value	Lack of fit *p*-value	C.V.%	Std. dev	Adeq. precision	R^2	Adjusted R^2	Predicted R^2	
Linear	0.0003	0.5210	14.88	8.77	9.0384	0.5823	0.4987	0.2087	Suggested
2FI	0.1897	0.5542	–	–	–	0.6385	0.5285	0.1756	Aliased

than 0.050. A, B, C, and E are important model terms in this instance. Model terms are not significant if the value is higher than 0.100. Model reduction may enhance this model if there are a lot of unnecessary words (except those needed to sustain the hierarchy). The *F*-value for the lack of fit, which is 1.11, indicates that the lack of fit is not significant in comparison to pure error. A significant Lack of Fit *F*-value has a 52.10% likelihood of being caused by noise. Non-significant lack of fit is beneficial since it demonstrates model fit (Zhang et al. 2010; Feilizadeh et al. 2015).

Following each experiment, the analysis focused on assessing the impacts of the variables to identify the optimum conditions for MNZ adsorption. The three-factor pair displays are shown in Fig. 12 (a–c). According to Sect. "Optimization of effective parameters on MNZ adsorption", MNZ adsorption efficiency increased with increasing adsorbent dose and decreasing MNZ concentration. This relationship also exists for decreasing pH and increasing adsorbent dose, while adsorption efficiency did not change noticeably and only slightly decreased concerning increasing temperature.

The response variable (MNZ degradation performance) was produced as a function of the five independent variables following the experimental design, and the resulting empirical linear coded equation is presented in Eq. (14).

$$\text{Removal Efficiency} = 38.16 + 9.72 * A - 8.75 * B - 16.25 * C + 0.4169 * D + 25.38 * E \quad (14)$$

The adjusted R^2 value of 0.4987 agrees rather well with the anticipated amount of R^2 of 0.2087. The average R^2 value suggests that the MNZ adsorption in the experimental range may be predicted using linear equations. Figure 13a compares the anticipated values of the final MNZ adsorption to the corresponding actual values. Additionally, Fig. 13b's depiction of the residuals' probability plot in standard form demonstrates that the assumptions are practically never violated: the errors exhibit a distribution that is typically homogeneous and independent, with equal variance (Zhang et al. 2010; Feilizadeh et al. 2019).

Regeneration and reusability of $AgZnFe_2O_4$@Ch

Economically and environmentally, the adsorption process depends on recovering and reusing the adsorbent. The magnetic nanocomposite $AgZnFe_2O_4$@Ch can be easily extracted from the media by a magnet and did not generate secondary contamination of the ecosystem of its high magnetic characteristics. To determine if the used nanoadsorbent could be reused, the adsorbent was separated from the process media utilizing a magnet, then heated to 200 °C for 10 min to eliminate the contaminants that had been adsorbed on it. Then, under optimal conditions, four recovery cycles were utilized to gauge its efficacy (Nasiri et al. 2022b). $AgZnFe_2O_4$@Ch, a magnetic nanocomposite, exhibited a diminish in adsorption efficiency across four cycles, from 65.53 to 61.74%. After four recovery cycles, as seen in Fig. 14 (MNZ: 10 mg/L, Adsorbent: 0.9 g/L), the adsorption

Table 6 ANOVA analysis for linear model

Source	Sum of squares	df	Mean square	*F*-value	*p*-value	
Model	2682.45	5	536.49	6.97	0.0003	Significant
A-adsorbent	601.85	1	601.85	7.82	0.0098	
B-MNZ concentration	417.19	1	417.19	5.42	0.0283	
C-pH	660.48	1	660.48	8.58	0.0072	
D-temperature	0.9848	1	0.9848	0.0128	0.9108	
E-time	1220.74	1	1220.74	15.86	0.0005	
Residual	1924.32	25	76.97			
Lack of fit	1641.41	21	78.16	1.11	0.5210	Not significant
Pure error	282.90	4	70.73			
Cor total	4606.76	30				

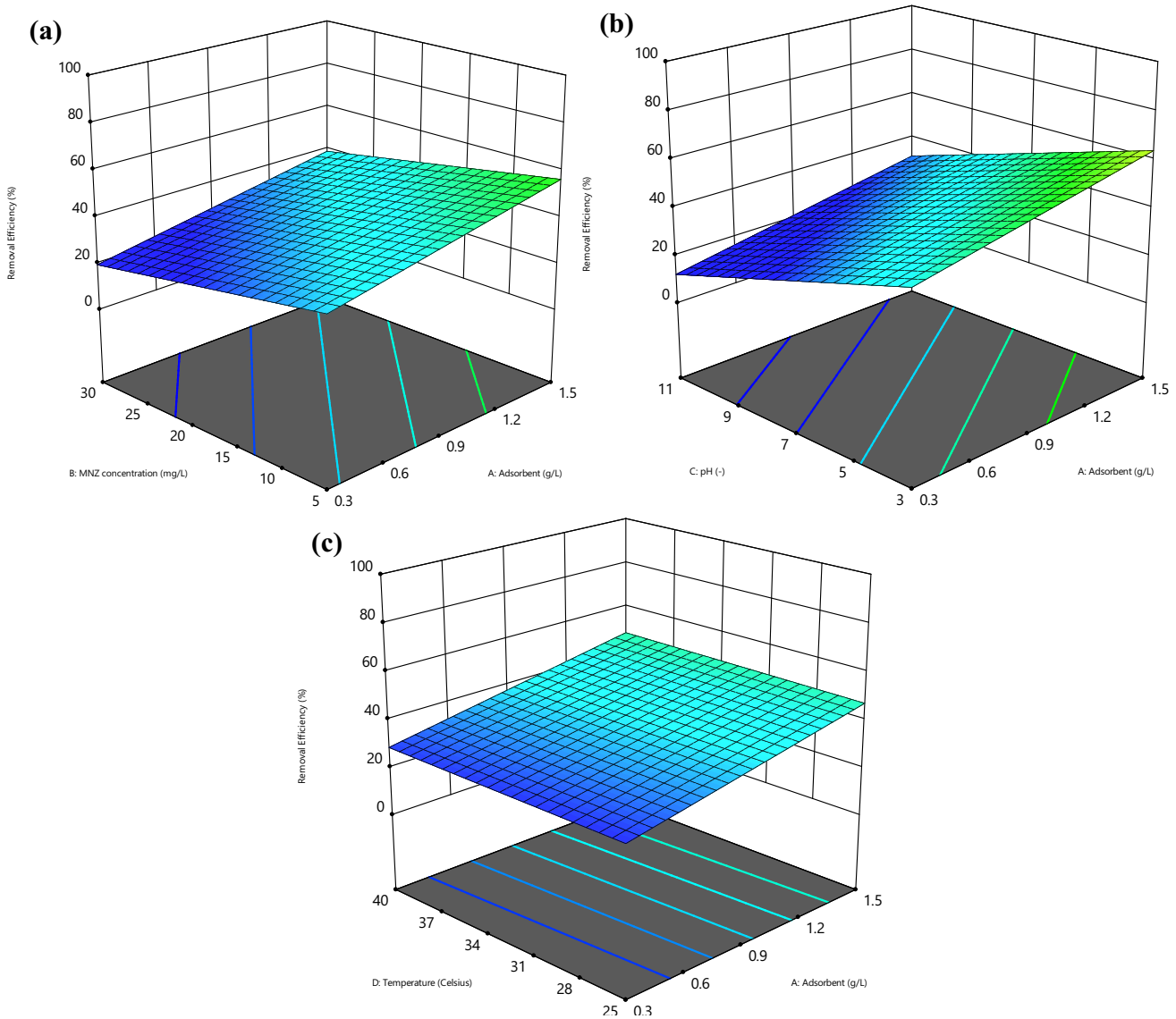

Fig. 12 Contour plots (**a**–**c**) for interaction between variables on MNZ adsorption

performance was 50%. This decrease in effectiveness may be brought on by the pollutant's presence in adsorbent sites, hence the reason for the loss in MNZ removal efficacy after four cycles of regeneration and reuse may be explained by the adsorbent's active sites becoming permanently occupied by the pollutant (Malakootian et al. 2019d).

Comparing MNZ adsorption with other adsorbents

According to Table 7, compared to other adsorbents, studied adsorbent is more practical, inexpensive, and efficient in removing. The surveys that were done to compare this study to other studies revealed that this study is more cost-effective concerning time and other factors.

Conclusion

The effectiveness of $AgZnFe_2O_4$@Ch for removing MNZ from aqueous solutions was examined in the current study, which involved the synthesis of the biocomposite adsorbent. The compositional impact of input elements and output response was studied using Design-Expert software. The selection of the linear model as an acceptable model for MNZ adsorption by $AgZnFe_2O_4$@Ch was made possible by its negligible lack of fit, lower *p*-value, and greater R^2 than the 2FI model. As a result, the adsorption process was predicted and optimized using this model. In terms of the coded factors, regression analysis of the linear model revealed that the variables adsorbent dosage, pH, MNZ concentration,

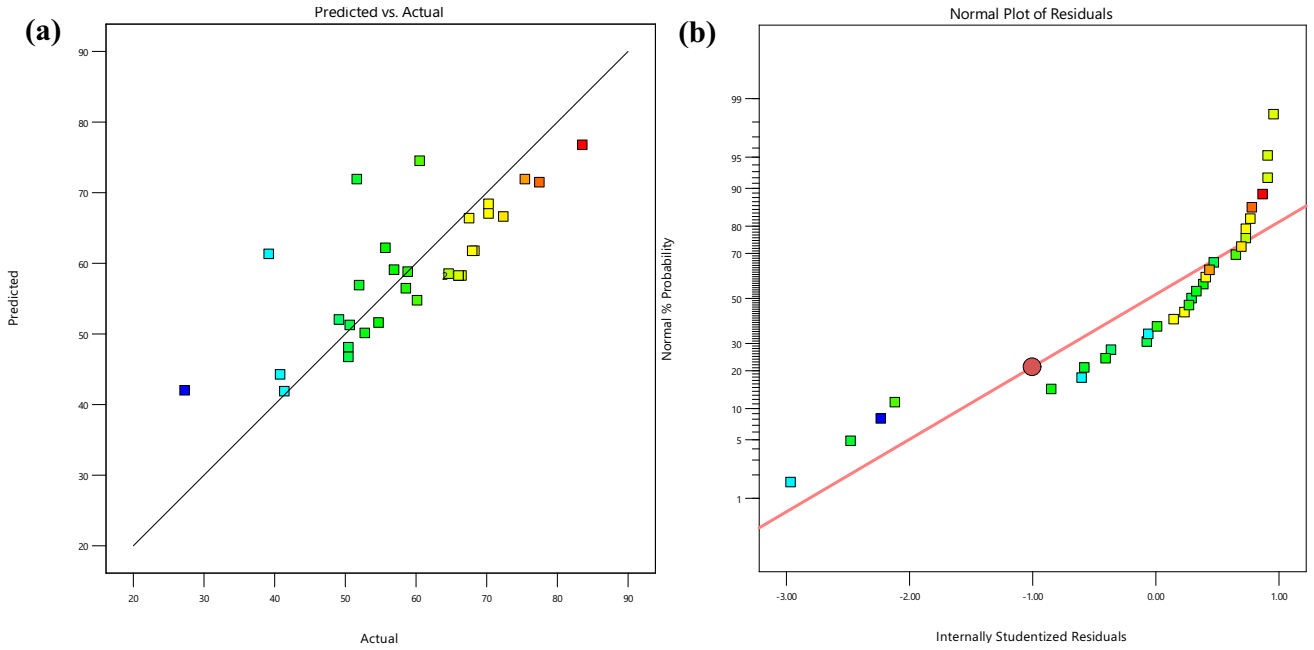

Fig. 13 Plots of the actual and predicted values (**a**) and the normal probability and internally studentized residuals (**b**) for the adsorption efficiency of MNZ

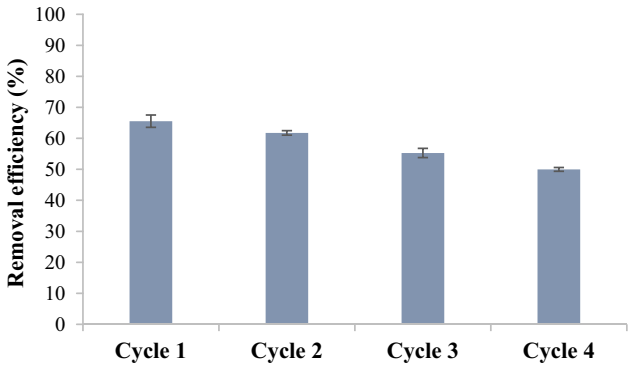

Fig. 14 Regeneration of $AgZnFe_2O_4$@Ch in the removal of MNZ (pH: 7, adsorbent: 0.9 g/L, MNZ initial concentration: 10 mg/L)

temperature, and time play essential roles in the adsorption process. According to the results, a single-layer method was involved in MNZ adsorption onto $AgZnFe_2O_4$@Ch. The Langmuir isotherm model was determined by the isotherm analysis to be the one that best explained the adsorption data. The MNZ adsorption on the $AgZnFe_2O_4$@Ch was found to be best described by the intraparticle kinetic model. Additionally, thermodynamic evaluations demonstrated that the MNZ adsorption on the $AgZnFe_2O_4$@Ch was exothermic and non-spontaneous. According to this study, MNZ could be effectively removed from hospital and industrial wastewater using $AgZnFe_2O_4$@Ch. It is advised that in further study, scientists compare these nanoparticles' effectiveness to that of other naturally occurring polysaccharides.

Table 7 Comparing $AgZnFe_2O_4$@Ch performance with other adsorbents

No	Adsorbent	Pollutant	Dose of adsorbent (g/L)	Initial concentration (mg/L)	Contact time (min)	Efficiency (%)	References
1	polyaniline-polypyrrole	Metronidazole	0.4	10	300	88.96	Aarab et al. (2020)
2	MgO/LECA	Metronidazole	1	40	150	97	s. (2017)
3	$FeNi_3/SiO_2/CuS$	Metronidazole	0.1	20	180	65.15	Nasseh et al. (2019)
4	Fe_3O_4@SiO_2-Chitosan/Graphene oxide	Tetracycline	0.4	44.4	480	85.7	Foroughi et al. (2020)
5	LDH	Tetracycline	6	60	150	82	Soori et al. (2016)
6	Biochar derived from sugarcane bagasse	Metronidazole	4	10	120	88.8	Sun et al. (2018)
7	$AgZnFe_2O_4$@Ch	Metronidazole	0.9	10	50	65.53	This work

Acknowledgements This research was conducted with project number 28060 and IR.SUMS.SCHEANUT.REC.1402.033 ethic approval cod in the Department of Environmental Health Engineering of Shiraz University of Medical Sciences.

Funding The author(s) received no specific funding for this work.

Declarations

Conflict of interest The authors affirm the absence of any known conflicting financial desires or personal relationships that might have seemed to impact the work disclosed in this manuscript.

References

Aarab N, Hsini A, Essekri A, Laabd M, Lakhmiri R, Albourine A (2020) Removal of an emerging pharmaceutical pollutant (metronidazole) using PPY-PANi copolymer: kinetics, equilibrium and DFT identification of adsorption mechanism. Groundw Sustain Dev 11:100416

Ahmed MJ, Theydan SK (2013) Microporous activated carbon from Siris seed pods by microwave-induced KOH activation for metronidazole adsorption. J Anal Appl Pyrol 99:101–109

Amiri Fard MH, Nasiri A, Daraei H (2023) Green synthesis of $AgCoFe_2O_4$@ Ch/AC as a recyclable, magnetic nanohybrid heterogeneous catalyst in photodegradation of ceftriaxone from aqueous solutions with effluent bioassay. Appl Water Sci 13(11):220

Amirmahani N, Mahdizadeh H, Seyedi N, Nasiri A, Yazdanpanah G (2023) Synthesis and performance evaluation of chitosan/zinc oxide nanocomposite as a highly efficient adsorbent in the removal of reactive red 198 from water. J Chin Chem Soc 70(4):869–878

Chavoshani A, Amin MM, Asgari G, Seidmohammadi A, Hashemi M (2018) Microwave/hydrogen peroxide processes. Elsevier, Advanced oxidation processes for waste water treatment, pp 215–255

de Carvalho OG, Filho GR, Vieira JG, De Assunção RMN, da Silva MC, Cerqueira DA et al (2010) Synthesis and application of methylcellulose extracted from waste newspaper in CPV-ARI Portland cement mortars. J Appl Polym Sci 118(3):1380–1385

El Bouraie MM, Ibrahim SS (2021) Comparative study between metronidazole residues disposal by using adsorption and photodegradation processes onto MgO nanoparticles. J Inorg Organomet Polym Mater 31(1):344–364

El-Sayed A (2002) Influence of zinc content on some properties of Ni–Zn ferrites. Ceram Int 28(4):363–367

Estahbanati MK, Feilizadeh M, Iliuta MC (2017) Photocatalytic valorization of glycerol to hydrogen: optimization of operating parameters by artificial neural network. Appl Catal B 209:483–492

Fadaei S, Moghadam FN, Hashemi M, Pourzamani H (2017) BTEX removal from aqueous solution by modified multi-walled carbon nanotubes with ozone. Anuario Do Instituto De Geociencias 40(1):235–242

Feilizadeh M, Mul G, Vossoughi ME (2015) coli inactivation by visible light irradiation using a Fe–Cd/TiO_2 photocatalyst: statistical analysis and optimization of operating parameters. Appl Catal B 168:441–447

Feilizadeh M, Attar F, Mahinpey N (2019) Hydrogen peroxide-assisted photocatalysis under solar light irradiation: interpretation of interaction effects between an active photocatalyst and H2O2. Can J Chem Eng 97(7):2009–2014

Fernandes Queiroz M, Melo KRT, Sabry DA, Sassaki GL, Rocha HAO (2015) Does the use of chitosan contribute to oxalate kidney stone formation? Mar Drugs 13(1):141–158

Firoozi M, Hashemi M, Narooie MR, Daraei H (2023) Evaluation of phenol degradation rate using advanced oxidation/reduction process (AO/RP) in the presence of sulfite and zinc oxide under UV. Optik 279:170787

Flores-Cano J, Sánchez-Polo M, Messoud J, Velo-Gala I, Ocampo-Pérez R, Rivera-Utrilla J (2016) Overall adsorption rate of metronidazole, dimetridazole and diatrizoate on activated carbons prepared from coffee residues and almond shells. J Environ Manage 169:116–125

Foroughi M, Azqhandi MHA, Kakhki S (2020) Bio-inspired, high, and fast adsorption of tetracycline from aqueous media using Fe_3O_4-g-CN@ PEI-β-CD nanocomposite: Modeling by response surface methodology (RSM), boosted regression tree (BRT), and general regression neural network (GRNN). J Hazard Mater 388:121769

Gharaghani MA, Samaei M, Mahdizadeh H, Nasiri A, Keshtkar M, Mohammadpour A et al (2024) An effective magnetic nanobiocomposite: preparation, characterization and its application for adsorption removal of P-nitroaniline from aquatic environments. Environ Res 246:118128

Ghiasi F, Solaimany Nazar AR, Farhadian M, Tangestaninejad S, Emami N (2022) Synthesis of aqueous media stable MIL101-OH/chitosan for diphenhydramine and metronidazole adsorption. Environ Sci Pollut Res 29(16):24286–24297

Guo L, Liang Y, Chen X, Xu W, Wu K, Wei H et al (2016) Effective removal of tetracycline from aqueous solution by organic acid-coated magnetic nanoparticles. J Nanosci Nanotechnol 16(3):2218–2226

Hashemi M, Amin MM, Sadeghi S, Menglizadeh N, Mohammadi F, Patastar S et al (2017) Coupling adsorption by NiO nanopowder with UV/H_2O_2 process for Cr (VI) removal. J Adv Environ Health Res 5(4):210–219

Hashemi H, Rajabi S, Nikooee S, Asrari E (2023) Ozonation of secondary industrial effluent for beneficial reuse. Desalin Water Treat 287:96–102

Hashemzadeh F, Derakhshandeh SH, Soori MM, Khedri F, Rajabi S (2023) Bisphenol A adsorption using modified aloe vera leaf-wastes derived bio-sorbents from aqueous solution: kinetic, isotherm, and thermodynamic studies. Int J Environ Health Res, 1–21

Ighalo JO, Igwegbe CA, Adeniyi AG, Adeyanju CA, Ogunniyi S (2020) Mitigation of Metronidazole (Flagyl) pollution in aqueous media by adsorption: a review. Environ Technol Rev 9(1):137–148

Javid N, Nasiri A, Malakootian M (2019) Removal of nonylphenol from aqueous solutions using carbonized date pits modified with ZnO nanoparticles. Desalin Water Treat 141:140–148

Kalhori EM, Al-Musawi TJ, Ghahramani E, Kazemian H, Zarrabi M (2017) Enhancement of the adsorption capacity of the light-weight expanded clay aggregate surface for the metronidazole antibiotic by coating with MgO nanoparticles: studies on the kinetic, isotherm, and effects of environmental parameters. Chemosphere 175:8–20

Karimi H, Mohammadi F, Rajabi S, Mahvi AH, Ghanizadeh G (2023) Biological 2, 4, 6-trinitrotoluene removal by extended aeration

activated sludge: optimization using artificial neural network. Sci Rep 13(1):9053
Liu T, Liu L, Gong X, Chi F, Ma Z (2021) Fabrication and comparison of active films from chitosan incorporating different spice extracts for shelf life extension of refrigerated pork. LWT 135:110181
Mahdizadeh H, Nasiri A, Gharaghani MA, Yazdanpanah G (2020) Hybrid UV/COP advanced oxidation process using ZnO as a catalyst immobilized on a stone surface for degradation of acid red 18 dye. MethodsX. 7:101118
Malakootian M, Dowlatshahi S, Hashemi CM (2013) Reviewing the photocatalytic processes efficiency with and without hydrogen peroxide in cyanide removal from aqueous solutions. J Mazandaran Univ Med Sci 23(104):69–78
Malakootian M, Nasiri A, Mahdizadeh H (2018a) Preparation of $CoFe_2O_4$/activated carbon@chitosan as a new magnetic nanobiocomposite for adsorption of ciprofloxacin in aqueous solutions. Water Sci Technol 78(10):2158–2170
Malakootian M, Hashemi M, Toolabi A, Nasiri A (2018b) Investigation of nickel removal using poly(amidoamine) generation 4 dendrimer (PAMAM G4) from aqueous solutions. J Eng Res (kuwait) 6(2):13–23
Malakootian M, Kannan K, Gharaghani MA, Dehdarirad A, Nasiri A, Shahamat YD et al (2019a) Removal of metronidazole from wastewater by Fe/charcoal micro electrolysis fluidized bed reactor. J Environ Chem Eng 7(6):103457
Malakootian M, Nasiri A, Alibeigi AN, Mahdizadeh H, Gharaghani MA (2019ab) Synthesis and stabilization of ZnO nanoparticles on a glass plate to study the removal efficiency of acid red 18 by hybrid advanced oxidation process (Ultraviolet/ZnO/ultrasonic). Desalin Water Treat 170:325–336
Malakootian M, Nasiri A, Khatami M, Mahdizadeh H, Karimi P, Ahmadian M et al (2019bc) Experimental data on the removal of phenol by electro-H2O2 in presence of UV with response surface methodology. MethodsX 6:1188–1193
Malakootian M, Nasiri A, Mahdizadeh H (2019cd) Metronidazole adsorption on $CoFe_2O_4$ /activated carbon@chitosan as a new magnetic biocomposite: modeling, analysis, and optimization by response surface methodology. Desalin Water Treat 164:215–227
Malakootian M, Nasiri A, Mahdizadeh H (2019de) Metronidazole adsorption on $CoFe_2O_4$/activated carbon@chitosan as a new magnetic biocomposite: modeling, analysis, and optimization by response surface methodology. Desalin Water Treat 164:215–227
Malakootian M, Nasiri A, Heidari MR (2019ef) Removal of phenol from steel plant wastewater in three dimensional electrochemical (TDE) process using $CoFe_2O_4$@AC/H_2O_2. Z Phys Chem 234(10):1661–1679
Malakootian M, Nasiri A, Asadipour A, Kargar E (2019fg) Facile and green synthesis of $ZnFe_2O_4$@ CMC as a new magnetic nanophotocatalyst for ciprofloxacin degradation from aqueous media. Process Saf Environ Prot 129:138–151
Malakootian M, Mahdizadeh H, Khavari M, Nasiri A, Gharaghani MA, Khatami M et al (2020) Efficiency of novel Fe/charcoal/ultrasonic micro-electrolysis strategy in the removal of acid red 18 from aqueous solutions. J Environ Chem Eng 8(2):103553
Malakootian M, Nasiri A, Heidari MR (2020a) Removal of phenol from steel plant wastewater in three dimensional electrochemical (TDE) process using CoFe2O4@AC/H2O2. Zeitschrift Fur Physikalische Chemie 234(10):1661–1679
Malakootian M, Smith A Jr, Gharaghani MA, Mahdizadeh H, Nasiri A, Yazdanpanah G (2020b) Decoloration of textile Acid Red 18 dye by hybrid UV/COP advanced oxidation process using ZnO as a catalyst immobilized on a stone surface. Desalin Water Treat 182:385–394
Maleky S, Asadipour A, Nasiri A, Luque R, Faraji M (2022) Tetracycline adsorption from aqueous media by magnetically separable Fe3O4@ Methylcellulose/APTMS: isotherm, kinetic and thermodynamic studies. J Polym Environ 30(8):3351–3367
Mallapur M, Shaikh P, Kambale R, Jamadar H, Mahamuni P, Chougule B (2009) Structural and electrical properties of nanocrystalline cobalt substituted nickel zinc ferrite. J Alloys Compd 479(1–2):797–802
Mehdinejad MH, Mengelizadeh N, Bay A, Pourzamani H, Hajizadeh Y, Niknam N et al (2018) Adsorption of methylene blue from aqueous solutions by cellulose and nanofiber cellulose and its electrochemical regeneration. Desalin Water Treat 110:250–263
Mohammadi F, Yavari Z, Rahimi S, Hashemi M (2019) Artificial neural network modeling of Cr (VI) biosorption from aqueous solutions. J Water Chem Technol 41(4):219–227
Morovati R, Ghaneian MT, Rajabi S, Dehghani M (2023a) Degradation efficiency of humic acid in presence of hydrogen peroxide and ultrasonic from aqueous media. Desalin Water Treat 281:249–254
Morovati R, Rajabi S, Ghaneian MT, Dehghani M (2023b) Efficiency of Ag_3PO_4/TiO_2 as a heterogeneous catalyst under solar and visible light for humic acid removal from aqueous solution. Heliyon 9(5):e15678
Naghizadeh M, Taher MA, Tamaddon A-M (2021) Application of $CoFe_2O_4$@ SiO_2@ chitosan nanoparticles for cadmium (ii) preconcentration in totally different samples and its determination through ETAAS. SILICON 13:3795–3806
Nasiri A, Tamaddon F, Mosslemin MH, Faraji M (2019) A microwave assisted method to synthesize nano$CoFe_2O_4$@methyl cellulose as a novel metal-organic framework for antibiotic degradation. MethodsX 6:1557–1563
Nasiri A, Malakootian M, Shiri MA, Yazdanpanah G, Nozari M (2021) CoFe2O4@methylcellulose synthesized as a new magnetic nanocomposite to tetracycline adsorption: modeling, analysis, and optimization by response surface methodology. J Polym Res 28(5):192
Nasiri A, Malakootian M, Heidari MR, Asadzadeh SN (2021) CoFe2O4@Methylcelloluse as a New Magnetic Nano Biocomposite for Sonocatalytic Degradation of Reactive Blue 19. J Polym Environ 29(8):2660–2675
Nasiri A, Rajabi S, Amiri A, Fattahizade M, Hasani O, Lalehzari A et al (2022a) Adsorption of tetracycline using $CuCoFe_2O_4$@ Chitosan as a new and green magnetic nanohybrid adsorbent from aqueous solutions: isotherm, kinetic and thermodynamic study. Arab J Chem 15(8):104014
Nasiri A, Rajabi S, Hashemi M, Nasab H (2022b) $CuCoFe_2O_4$@ MC/AC as a new hybrid magnetic nanocomposite for Metronidazole removal from wastewater: bioassay and toxicity of effluent. Sep Purif Technol 296:121366
Nasiri A, Rajabi S, Hashemi M (2022c) $CoFe_2O_4$@ methylcellulose/AC as a new, green, and eco-friendly nano-magnetic adsorbent for removal of reactive red 198 from aqueous solution. Arab J Chem 15(5):103745
Nasiri A, Golestani N, Rajabi S, Hashemi M (2024) Facile and green synthesis of recyclable, environmentally friendly, chemically stable, and cost-effective magnetic nanohybrid adsorbent for tetracycline adsorption. Heliyon.
Nasseh N, Barikbin B, Taghavi L, Nasseri MA (2019) Adsorption of metronidazole antibiotic using a new magnetic nanocomposite from simulated wastewater (isotherm, kinetic and thermodynamic studies). Compos B Eng 159:146–156
Oliveira RL, Vieira JG, Barud HS, Assunção RMN, Rodrigues Filho G, Ribeiro SJL et al (2015) Synthesis and characterization of methylcellulose produced from bacterial cellulose under heterogeneous condition. J Braz Chem Soc 26:1861
Pezeshki H, Hashemi M, Rajabi S (2023) Removal of arsenic as a potentially toxic element from drinking water by filtration: a mini review of nanofiltration and reverse osmosis techniques. Heliyon 9(3):e14246

Pourshaban-Mazandarani M, Ahmadian M, Nasiri A, Poormohammadi A (2023) $CuCoFe_2O_4$@ AC magnetic nanocomposite as a novel heterogeneous Fenton-like nanocatalyst for Ciprofloxacin degradation from aqueous solutions. Appl Water Sci 13(9):179

Pourzamani H, Parastar S, Hashemi M (2017) The elimination of xylene from aqueous solutions using single wall carbon nanotube and magnetic nanoparticle hybrid adsorbent. Process Saf Environ Prot 109:688–696

Pourzamani H, Hashemi M, Bina B, Rashidi A, Amin MM, Parastar S (2018) Toluene removal from aqueous solutions using single-wall carbon nanotube and magnetic nanoparticle–hybrid adsorbent. J Environ Eng 144(2):04017104

Rahmani A, Mengelizadeh N, Darvishmotevalli M, Salari M, Moradnia M, Noorisepehr M, et al. (2022) Effective degradation of amoxicillin using peroxymonosulfate activated with MWCNTs-CuNiFe2O4 as a new catalyst: optimization, degradation pathway, and toxicity assessment. Biomass Conversion and Biorefinery. 1–14

Rajabi S, Nasiri A, Hashemi M (2022) Enhanced activation of persulfate by $CuCoFe_2O_4$@MC/AC as a novel nanomagnetic heterogeneous catalyst with ultrasonic for metronidazole degradation. Chemosphere 286(3):131872

Sadeghi S, Raki G, Amini A, Mengelizadeh N, Amin MM, Hashemi M (2018) Study of the effectiveness of the third generation polyamideamine and polypropylene imine dendrimers in removal of reactive blue 19 dye from aqueous solutions. Environ Health Eng Manag J 5(4):197–203

Sekiguchi Y, Sawatari C, Kondo T (2003) A gelation mechanism depending on hydrogen bond formation in regioselectively substituted O-methylcelluloses. Carbohyd Polym 53(2):145–153

Shahrezaei F, Mansouri Y, Zinatizadeh AAL, Akhbari A (2012) Process modeling and kinetic evaluation of petroleum refinery wastewater treatment in a photocatalytic reactor using TiO_2 nanoparticles. Powder Technol 221:203–212

Sharifi N, Nasiri A, Martínez SS, Amiri H (2022) Synthesis of Fe_3O_4@ activated carbon to treat metronidazole effluents by adsorption and heterogeneous fenton with effluent bioassay. J Photochem Photobiol, A 427:113845

Soori MM, Ghahramani E, Kazemian H, Al-Musawi TJ, Zarrabi M (2016) Intercalation of tetracycline in nano sheet layered double hydroxide: an insight into UV/VIS spectra analysis. J Taiwan Inst Chem Eng 63:271–285

Sun L, Chen D, Wan S, Yu Z (2018) Adsorption studies of dimetridazole and metronidazole onto biochar derived from sugarcane bagasse: kinetic, equilibrium, and mechanisms. J Polym Environ 26(2):765–777

Tamaddon F, Mosslemin MH, Asadipour A, Gharaghani MA, Nasiri A (2020) Microwave-assisted preparation of $ZnFe_2O_4$@methyl cellulose as a new nano-biomagnetic photocatalyst for photodegradation of metronidazole. Int J Biol Macromol 154:1036–1049

Varma R, Vasudevan S (2020) Extraction, characterization, and antimicrobial activity of chitosan from horse mussel modiolus modiolus. ACS Omega 5(32):20224–20230

Wiercigroch E, Szafraniec E, Czamara K, Pacia MZ, Majzner K, Kochan K et al (2017) Raman and infrared spectroscopy of carbohydrates: a review. Spectrochim Acta Part A Mol Biomol Spectrosc 185:317–335

Yakoubi S, Kobayashi I, Uemura K, Nakajima M, Isoda H, Ksouri R et al (2021) Essential-oil-loaded nanoemulsion lipidic-phase optimization and modeling by response surface methodology (RSM): enhancement of their antimicrobial potential and bioavailability in nanoscale food delivery system. Foods 10(12):3149

Yazdanpanah G, Heidari MR, Amirmahani N, Nasiri A. (2023) Heterogeneous Sono-Fenton like catalytic degradation of metronidazole by Fe3O4@ HZSM-5 magnetite nanocomposite. Heliyon, 9(6)

Yurtay A, Kılıç M (2023) Biomass-based activated carbon by flash heating as a novel preparation route and its application in high efficiency adsorption of metronidazole. Diam Relat Mater 131:109603

Zhang J, Fu D, Xu Y, Liu C (2010) Optimization of parameters on photocatalytic degradation of chloramphenicol using TiO_2 as photocatalyist by response surface methodology. J Environ Sci 22(8):1281–1289

Zhu X, He M, Sun Y, Xu Z, Wan Z, Hou D et al (2022) Insights into the adsorption of pharmaceuticals and personal care products (PPCPs) on biochar and activated carbon with the aid of machine learning. J Hazard Mater 423:127060